Cold Regions Science and Technology 183 (2021) 103233

Contents lists available at ScienceDirect

Cold Regions Science and Technology

journal homepage: www.elsevier.com/locate/coldregions

Energy and mass balance dynamics of the seasonal snowpack at two high-altitude sites in the Himalaya

Emmy E. Stigter [a,*], Jakob F. Steiner [a], Inka Koch [b,c], Tuomo M. Saloranta [d], James D. Kirkham [b,e,f], Walter W. Immerzeel [a]

[a] Utrecht University, Department of Physical Geography, Princetonlaan 8a, 3584CB, Utrecht, the Netherlands
[b] International Centre for Integrated Mountain Development, Khumaltar, Lalitpur, Kathmandu, G.P.O. Box 3326, Nepal
[c] Department of Geosciences, University of Tübingen, Schnarrenbergstr. 94-96, 72076 Tübingen, Germany
[d] Norwegian Water Resources and Energy Directorate, Hydrology department, Postboks 5091, Majorstua 0301, Oslo, Norway
[e] Scott Polar Research Institute, University of Cambridge, Lensfield Road, Cambridge CB2 1ER, United Kingdom
[f] British Antarctic Survey, Natural Environment Research Council, High Cross, Madingley Road, Cambridge CB3 0ET, United Kingdom

ARTICLE INFO

Keywords:
Refreezing
Snowpack cold content
Snowmelt
Snowpack energy balance
Himalaya

ABSTRACT

Snow dynamics play a crucial role in the hydrology of alpine catchments in the Himalaya. However, studies based on in-situ observations that elucidate the energy and mass balance of the snowpack at high altitude in this region are scarce. In this study, we use meteorological and snow observations at two high-altitude sites in the Nepalese Himalaya to quantify the mass and energy balance of the seasonal snowpack. Using a data driven experimental set-up we aim to understand the main meteorological drivers of snowmelt, illustrate the importance of accounting for the cold content dynamics of the snowpack, and gain insight into the role that snow meltwater refreezing plays in the energy and mass balance of the snowpack. Our results show an intricate relation between the sensitivity of melt and refreezing on the albedo, the importance of meltwater refreezing, and the amount of positive net energy used to overcome the cold content of the snowpack. The net energy available at both sites is primarily driven by the net shortwave radiation, and is therefore extremely sensitive to snow albedo measurements. We conclude that, based on observed snowpack temperatures, 21% of the net positive energy is used to overcome the cold content build up during the night. We also show that at least 32–34% of the snow meltwater refreezes again for both sites. Even when the cold content and refreezing are accounted for, excess energy is available beyond what is needed to melt the snowpack. We hypothesize that this excess energy may be explained by uncertainties in the measurement of shortwave radiation, an underestimation of refreezing due to a basal ice layer, a cold content increase due to fresh snowfall and the ground heat flux. Our study shows that in order to accurately simulate the mass balance of seasonal snowpacks in Himalayan catchments, simple temperature index models do not suffice and refreezing and the cold content needs to be accounted for.

1. Introduction

Snow in alpine catchments is a seasonal water storage that strongly influences catchment hydrology. The quantification of the timing and volume of snow meltwater is essential for irrigation, hydropower and flood and drought risk assessment.

Snowpack dynamics in the Himalaya have been scarcely studied based on in situ observations (Kirkham et al., 2019). Typically, snow studies in this region rely heavily on satellite remote sensing, modelling, or a combination of both (e.g. Bookhagen and Burbank, 2010; Immerzeel et al., 2009; Lievens et al., 2019; Smith et al., 2017; Smith and Bookhagen, 2018). Remote sensing products provide mainly information on snow cover, but do not provide information about the energy and mass balance of the snowpack. Recent progress has been made in improving the vertical resolution of remotely sensed snow products. Smith and Bookhagen (2018) developed a remotely sensed snow water equivalent (SWE) product from passive microwave data from 1987 until 2009. However, its absolute SWE values are unreliable and hence only relative changes have been investigated to study trends on the scale of High Mountain Asia (Smith and Bookhagen, 2018). In addition, the

* Corresponding author.
E-mail address: e.e.stigter@uu.nl (E.E. Stigter).

https://doi.org/10.1016/j.coldregions.2021.103233
Received 10 June 2020; Received in revised form 17 December 2020; Accepted 11 January 2021
Available online 15 January 2021

coarse spatial resolution of this product fails to capture the high heterogeneity of snow processes and properties. Another study by Lievens et al. (2019) derived snow depth at a relatively high spatial resolution (1 km^2) from Sentinel-1 satellite data for all mountain ranges in the Northern Hemisphere. Even though this new product is promising to study snow depth variability, the scarcity of validation sites in the Himalaya precludes proper evaluation of this product in this region (Lievens et al., 2019). Besides remotely sensed snow products, models are used to understand the energy and mass balance of a snowpack. Snowmelt simulations can be performed with models of different complexity. In Himalayan snow studies, where data availability is low, the simple degree-day method and the Enhanced-Temperature Index (ETI) method are primarily used (Bookhagen and Burbank, 2010; Ragettli et al., 2015; Saloranta et al., 2019; Stigter et al., 2017). In contrast, physically-based snow models that include a full energy balance approach (e.g. Bartelt and Lehning, 2002; Vionnet et al., 2012) are more complex and have higher data requirements, which are often not available in a Himalayan context (c.f. Bolch et al., 2019). However, simplistic snowmelt models generally do not account for snow processes, such as refreezing, sublimation and wind redistribution, that can be important at high altitude, where snow ablation is not necessarily dominated by melt (Litt et al., 2019; Stigter et al., 2018). Another limitation of these models is that they simulate snowmelt runoff as soon as temperatures rise above the threshold temperature for melt onset. However, melting of a snowpack consists of three phases: i) the warming phase in which absorbed energy raises the average snowpack temperature to an isothermal temperature of 0 °C, ii) the ripening phase in which snow melts but the meltwater is retained within the snowpack in the pore spaces, and iii) the output phase when snowmelt drains from the snowpack as result of additional absorbed energy (Dingman, 2008). These phases alternate at both seasonal and daily time scales as a result of periods with repeated negative net energy, which leads to the cooling of the snowpack and refreezing of meltwater retained within the snowpack. These may be important processes as this potentially leads to the same snow being warmed and melted multiple times before the end of the snow season, resulting in a delay in snowmelt onset and runoff (e.g. Bengtsson, 1982a, 1982b; Jennings et al., 2018; Pfeffer et al., 1991; Pfeffer and Humphrey, 1998). Several studies have shown that sub-daily runoff simulations are improved by using an energy balance approach instead of the degree-day method in alpine terrain as the more sophisticated energy balance approach accounts for the different phases of snowmelt (Avanzi et al., 2016; Förster et al., 2014; Warscher et al., 2013).

Refreezing of snow meltwater, retained within the snowpack, can have a considerable effect on the energy and mass balance of a snowpack. Although refreezing has been extensively studied at high latitudes (e.g. van Pelt et al., 2016; Van Pelt et al., 2012; Reijmer et al., 2012; Steger et al., 2017), this process has attained little attention at lower latitudes (Samimi and Marshall, 2017). Mölg et al. (2012) and Fujita and Ageta (2000) estimated that a considerable amount of snow meltwater

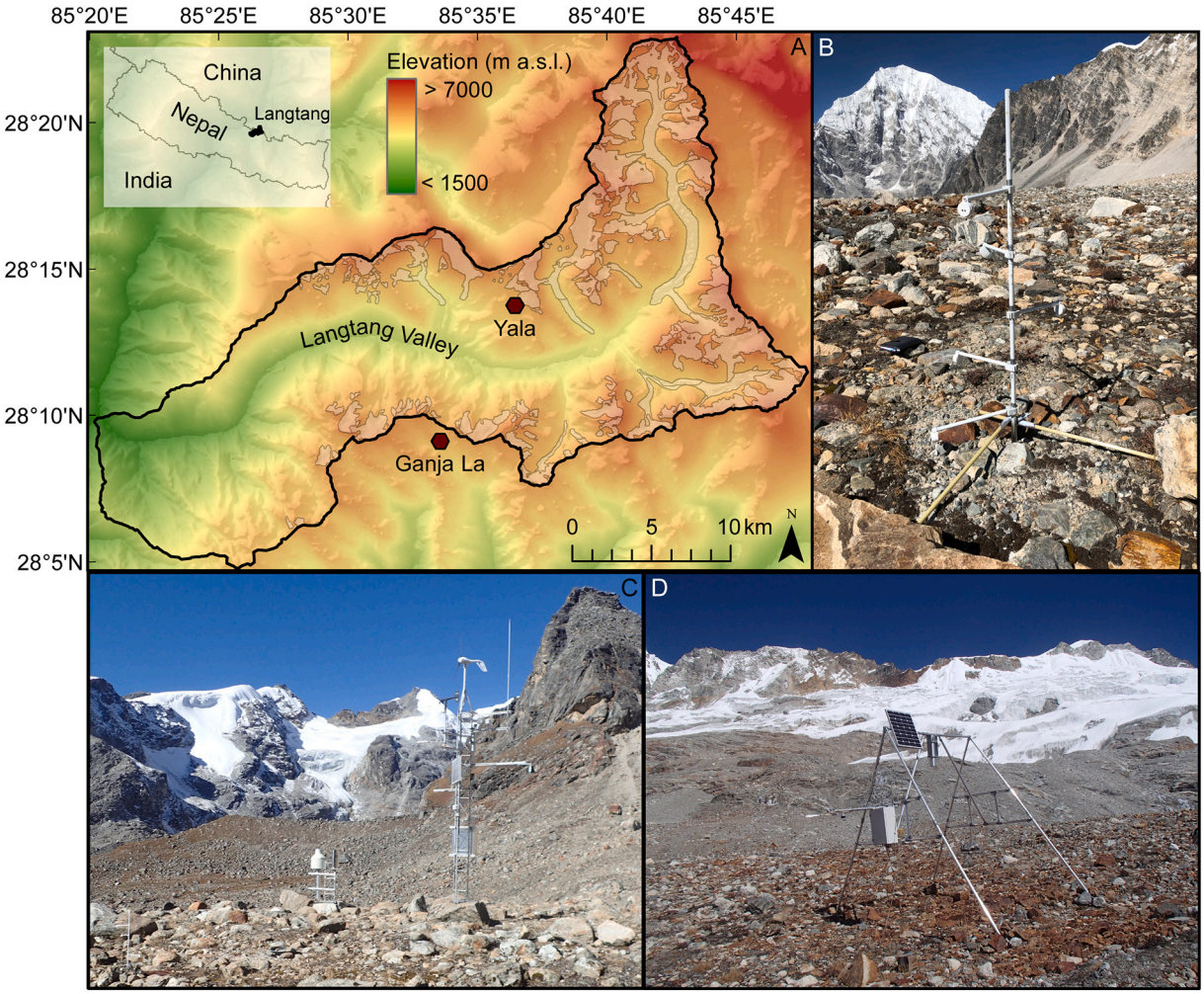

Fig. 1. Panel A gives an overview of the location of the Langtang Valley and the locations of the two sites (Yala and Ganja La). The white outlines indicate the extent of the glaciers located within the valley. Panel B shows the measurement set-up of the vertical snow temperature profile at Yala (Section 3.2). Panels C and D show the automatic weather stations with the CS725 SWE sensors and the surrounding terrain at Ganja La and Yala, respectively.

refreezes, 13 and 20% respectively, on two glaciers on the Tibetan Plateau, using an energy-balance model. Only Saloranta et al. (2019) made a first order approximation of the importance of refreezing in a Himalayan catchment. They estimated that 36% of the meltwater, simulated by an ETI-model, refreezes.

Based on an extensive set of meteorological and snow observations at two high-altitude sites in the Himalaya, we will quantify the mass and energy balance of the seasonal snowpack, illustrate the importance of refreezing, and elucidate cold content dynamics of the snowpack.

2. Study area

The Langtang Valley is located in the Central Himalaya in Nepal (Fig. 1). The elevation ranges between 1500 m a.s.l. and 7140 m a.s.l. for the highest peak, Langtang-Lirung. In this valley, an extensive set of snow and meteorological measurements was collected at two high-altitude sites, Ganja La (N28.1545, E85.5625) and Yala (N28.2323, E85.6097), at ~4962 and 5090 m a.s.l., located at the southern and northern sides of the valley, respectively (Fig. 1). The climate is monsoon dominated with most precipitation (up to 84%) falling from June to September as rain (Immerzeel et al., 2014; Kirkham et al., 2019). Westerlies transport moist air into the valley during winter, resulting in snowfall at the two high-altitude sites forming a snowpack. The snowpack is typically shallow in the winter months (November-February) based on only a few snowfall events and further accumulates from March until May (Kirkham et al., 2019; Saloranta et al., 2019). Although the sites are only approximately 15 km apart and have generally the same climatic regime, there are distinct differences in the wind, atmospheric moisture and radiation regimes as Ganja La is located south of the water divide, which acts as a topographic barrier.

3. Data and methodology

In this study the main focus is on the snow-covered period in 2018 at Ganja La (5 March-25 May) and Yala (9 February-26 May) when meteorological and snow observations were recorded at both sites and captured the full snow season. In order to show interannual variability, data from the Ganja La site was also analyzed for the snow-covered periods in 2017 (27 January-15 May) and 2019 (15 February-10 June).

3.1. Meteorological observations

Two automatic weather stations (AWS) recorded hourly meteorological observations at the Ganja La and Yala sites (Fig. 1). The observed variables include incoming and outgoing shortwave and longwave radiation, wind speed and direction, air temperature, relative humidity and atmospheric pressure (Table 1).

3.2. Snow observations

A Campbell Scientific CS725 sensor provided automated measurements of the SWE at both sites (Table 1). The CS725 passively measures the emitted electromagnetic radiation from the decay of naturally existing radioactive potassium and thallium in the soil. This signal is attenuated due to accumulation of snow; the attenuation of measured electromagnetic energy is then used to calculate SWE. The CS725 measures over a 24-h window to detect a sufficient amount of emitted electromagnetic radiation, which is reported every 6 h. The 6-h records of SWE were linearly interpolated to obtain the same hourly temporal resolution as the meteorological observations. In addition, an 18-h time lag was applied to the SWE time series, in accordance with the findings of Kirkham et al. (2019). The footprint of the sensor is a function of the sensor height, i.e. ~150 m^2 and 85 m^2 at the Ganja La and Yala sites, respectively. The accuracy of the measurements is ±15 mm from 0 to 300 mm and ± 15% from 300 to 600 mm. Snow accumulation exceeding 600 mm results in considerable errors.

Table 1
Description and specifications of the sensors at the locations Ganja La and Yala.

Sensor	Variable	Accuracy	Sensor height [m]
Ganja La			
Campbell Scientific CS725	SWE	±15 mm/ ±15%	4.00
Young Wind Monitor-HD-Alpine 5108–45	Wind speed, wind direction	±0.3 m s^{-1}, ±3°	4.46
Campbell Scientific CS215	Relative humidity	±4%	2.09
Campbell Scientific SR50A-316SS	Air temperature	±0.2 °C	3.40
Sutron 5600–0120-3C	Atmospheric pressure	±0.4 hPa	0.80
Kipp&Zonen CNR4 Net Radiometer	Incoming/outgoing longwave/shortwave radiation	±3%	3.54
Yala			
Campbell Scientific CS725	SWE	±15 mm/ ±15%	2.98
Young Wind Monitor 05103	Wind speed, wind direction	±0.3 m s^{-1}/ ±3°	2.50
Campbell Scientific HC2S3	Air temperature, relative humidity	±0.1 °C/ ±0.8%	1.75
Campbell Scientific CS106	Atmospheric pressure	±1.0 hPa	0.80
Kipp&Zonen CNR4 Net Radiometer	Incoming/outgoing longwave/shortwave radiation	±3%	2.20
HOBO TidbiT v2	Snow temperature	±0.2 °C	0.0, 0.15, 0.30, 0.45, 0.60

Besides the SWE observations, automated measurements of the vertical snow temperature profiles were measured at the Yala site at approximately 5-m distance from the CS725 (Fig. 1). Temperature sensors (TidbiT) recorded the snow temperature at 15-min intervals and were positioned at 0, 15, 30, 45 and 60 cm above the snow-ground interface. The observations were aggregated to hourly means to match the temporal resolution of the meteorological observations. The temperature sensors were painted white to reduce the influence of direct radiative warming. The vertical temperature profile provides valuable information on the development of the cold content of the snowpack and the onset of snowmelt. A time-lapse camera provided hourly pictures of the set-up at Yala during the day, which was used to determine whether the temperature sensors were covered by snow. The time lapse imagery was also used to interpret and quality-check the observed time series of the SWE and to evaluate the patchiness of the snow cover.

3.3. Surface energy balance

The net energy (E_{net}) at the snow surface was calculated as the sum of the radiative and turbulent fluxes (all in W m^{-2}; Eq. (1)):

$$E_{net} = S_{net} + L_{net} + H + LE \quad (1)$$

where S_{net} and L_{net} are the net incoming shortwave and longwave radiation respectively, H is the sensible heat flux and LE is the latent heat flux. Fluxes pointing towards the surface are assumed positive whereas fluxes pointed towards the atmosphere are negative. Heat advection by precipitation has in general a negligible influence on the energy balance of a snowpack, especially in climates with relatively little accumulation (e.g. Marks and Dozier, 1992). Therefore, heat advection by precipitation was neglected in the calculations of the surface energy balance. The ground heat flux was also excluded in this study as adequate observations of the ground heat flux are non-existing in the Himalaya and therefore its magnitude and potential role in the energy balance remains unknown.

The hourly S_{net} was calculated from the hourly observed incoming shortwave radiation multiplied with the albedo at 12 h, when the solar

zenith angle is small. The albedo is inferred from the incoming and outgoing shortwave radiation measurements. However, the albedo was set to a minimum value of 0.46 and 0.41 to exclude the influence of snow patchiness on the observed albedo at the end of the snow season for the Ganja La and Yala sites, respectively. Kirkham et al. (2019) estimated the minimum albedo of continuous snow cover at Ganja La as 0.46. For Yala, the minimum albedo was determined by taking the albedo on the last day that snow cover was continuous (observed using time-lapse imagery). In addition, observations of incoming shortwave radiation at Yala were replaced with observations from a nearby station, located at the same elevation and at 150 m distance (AWS Yala BC; see Shea et al. (2015a) for details), when the measurements of incoming shortwave radiation were influenced by shading of the station structure itself. This mainly occurred in April and May between 7 and 9 h.

L_{net} was calculated as the difference between the observed incoming and outgoing longwave radiation. The turbulent fluxes were calculated using the bulk-aerodynamic method, explained in detail in Stigter et al. (2018) and (Litt et al., 2015). Stigter et al. (2018) calibrated the roughness lengths for momentum, heat and humidity ($1.3*10^{-3}$ m, $1.3*10^{-4}$ m and $1.3*10^{-4}$ m, respectively) using observed turbulent fluxes with an eddy covariance system on the nearby Yala Glacier, which was snow-covered during the observation period. We used these roughness lengths to calculate the turbulent fluxes at the two sites.

3.4. Mass balance

The change in the mass balance of the snowpack ($\Delta mass$) was calculated as the sum of melt, refreezing (*refr*), sublimation (*subl*), evaporation (*evap*), deposition (*dep*), snowfall (*snow*), rainfall (in case of rain-on-snow; *rain*) and redistribution by wind (*red*) at an hourly time step (all in mm; Eq. (2)):

$$\Delta mass = melt + refr + subl + evap + dep + snow + rain + red \quad (2)$$

Mass losses were assumed negative, whereas mass gains were positive. Gains in mass by snowfall, rain-on-snow and wind redistribution were merged and derived from increases in the SWE in the CS725 data. Decreases in SWE due to wind redistribution are difficult to derive from the SWE data because decreases in SWE can be a result of both melt and snow erosion by wind, which may both occur during the 24-h measurement interval. Snow erosion by wind has likely only a minor influence on the mass balance, as both locations are relatively sheltered, and especially at Ganja La the wind speed is generally low (< 2 m s^{-1}). In addition, the footprint of the SWE measurements is relatively large at both sites (85 and 150 m^2), and snow eroded within the footprint may also be deposited within the footprint, resulting in no net change in observed SWE. Therefore, we did not account for mass losses due to wind redistribution in this study.

3.5. Snowpack energy balance experiments

Refreezing of meltwater and especially the cold content dynamics of the snowpack are commonly ignored in melt models applied in the Himalaya (e.g. Immerzeel et al., 2012; Ragettli et al., 2015; Saloranta et al., 2019; Shea et al., 2015b; Stigter et al., 2017). We conducted four energy balance experiments using data of the 2018 winter snow season (February until May), with varying assumptions, to quantify the importance of the snowpack's cold content and refreezing of meltwater for the energy and mass balance of the snowpack. The snowpack energy balance experiments in this study are all based on the observed surface energy balance. However, we partitioned the positive net energy at the surface between energy used for warming and energy used for melt of the snowpack, based on applying a threshold value of 0 °C for the surface temperature (derived from the measured outgoing longwave radiation using the Stefan Boltzmann law). Negative net energy at the surface is either used for cooling of the snowpack or for refreezing of meltwater stored in the snowpack. Cooling of the snowpack only occurs once all meltwater, stored within the snowpack, has refrozen. Consequently, net energy at the snow surface is the same for all experiments. However, the assumption regarding how this energy is used for melting, refreezing or cooling or warming of the snowpack varies among the experiments. The experiments are explained in more detail below. All energy balance calculations were performed as long as the observed SWE exceeded 15 mm, which equals the accuracy of the CS725 (Table 1).

Exp. 1 No cold content and no refreezing
: It was assumed that all net positive energy is used for melt in this first experiment. Both the cold content of the snowpack and refreezing of liquid water in the snowpack were not accounted for and it was assumed that all meltwater directly runs off.

Exp. 2 Cold content and no refreezing
: In this experiment it was assumed that all net negative energy is used for cooling of the snowpack. If the net energy is positive, it is first used to warm the snowpack as long as the surface temperature is below the melting point (0 °C). All remaining positive energy is used for melt, which was assumed to run off directly.

Exp. 3 Cold content and unlimited refreezing
: In this experiment, similar to Exp. 2, all positive net energy is first used to warm the snowpack until the surface temperature is 0 °C. All remaining positive energy is used for melt. If the net energy is negative, this energy is directed to refreezing, assuming unlimited availability of water.

Exp. 4 Cold content and water limited refreezing
: In this experiment, similar to Exp. 2 and 3, all positive net energy is first used to warm the snowpack until the surface temperature is 0 °C. All remaining positive energy is used for melt. The meltwater is now however retained within the snowpack as long as the water content is lower than 10% of the observed SWE. This 10% of SWE corresponds to a volume % of 1.4–4.6, which, given a range in bulk snow density between 150 and 550 kg m^{-3}, is a plausible estimate (Heilig et al., 2015; Samimi and Marshall, 2017; Wever et al., 2015). If the net energy is negative, this energy is used for refreezing as long as liquid water is available in the snowpack. After all available water has refrozen, this negative energy was assumed to cool down the snowpack and increase the cold content.

Using this experimental set-up it is possible to quantify: i) how much of the net positive energy is used for overcoming the cold content of the snowpack (by comparing Exp. 1 and 2), ii) the upper limit of the amount of net negative energy that may be used for refreezing (by comparing Exp. 2 and 3), and iii) how much energy is used for refreezing when the amount of liquid water in the snowpack is realistically constrained by a maximum storage capacity (by comparing Exp. 3 and 4).

3.6. Observed vertical snow temperature profile and cold content of the snowpack

In the experimental set-up described above, the cold content is derived based on the surface energy balance. However, the cold content can also be derived independently using the snow temperature measurements inside the snowpack. The observation-based cold content of the snowpack (CC, J m^{-2}) was calculated using the observations of SWE (m) and average snowpack temperature (T_{snow}, °C), based on the observed vertical snow temperature profile (Eq. (3)):

$$CC = -c_i \rho_w SWE (T_{snow} - T_{melt}) \quad (3)$$

Where c_i is the heat capacity of ice (2102 J kg^{-1} $°C^{-1}$), ρ_w is the density of water (1000 kg m^{-3}) and T_{melt} is the melting temperature of snow (0 °C). Warming and cooling of the snowpack was calculated based

on changes in the average snowpack temperature and therefore its cold content.

4. Results

4.1. Observed meteorology and SWE

The 2018 winter season has a continuous time series of SWE at both sites, Ganja La and Yala. There is a persistent (SWE > 15 mm) snowpack from March 2018 until May 2018 at Ganja La for this season, and from February 2018 until May 2018 at Yala (Fig. 2). The accumulation of SWE is generally higher at Yala compared to Ganja La, even though the sites only differ slightly in altitude. The SWE time series show large inter-annual variability of the snow accumulation at both sites, with approximately three times higher maximum accumulation in 2019 than in 2018 (Fig. 2).

There are clear meteorological differences between Yala and Ganja La when snow is present during the 2018 winter season (Fig. 3). Fig. 3 shows differences in the observed wind speed and relative humidity between the two sites. The relative humidity increases at approximately 8 h at Ganja La, whereas it increases at approximately 13–14 h at Yala. At Ganja La, the wind speed is generally low and has no distinct diurnal cycle, whereas at Yala the wind speed has a strong diurnal cycle with higher wind speeds occurring in the afternoon during the entire snow season, potentially linked in with the overall valley circulation. These differences in wind speed are likely a result of the complex interaction between the catchment topography, katabatic and synoptic scale wind patterns.

The surface temperature and air temperature show similar diurnal cycles with equal magnitude at both locations (Fig. 3). The surface temperature remains below freezing point from February to March at Yala, whereas the surface temperature already reaches 0 °C at Ganja La in March. The surface temperature shows a gradual shift throughout the snow season towards longer time periods with the surface being at melting point at both sites (Fig. 3). The snow surface is at melting point for approximately 4–5 h during the day in May, whereas this is roughly 2 h in April on average. The surface temperature occasionally reaches values above 0 °C in May. This is a result of boulders protruding the snow cover within the footprint of the sensor that can have a higher temperature than a melting snow surface (0 °C). However, we believe this influence is restricted to late melt season only, when the snowpack is very shallow. The air temperature is consistently higher than the surface temperature during night at Ganja La and Yala for the entire snow season, which is indicative of a positive sensible heat flux. However, at Ganja La the air temperature is considerably lower than the surface temperature from approximately 10 h to 15 h in March and April, whereas at Yala the air temperature is only slightly lower or equal to the surface temperature during daytime.

4.2. Surface energy balance characterization of the 2018 winter period

Fig. 4 shows the measured hourly radiative balance and the calculated turbulent fluxes for the two sites Ganja La and Yala for the months February to May 2018 when a snowpack is present. The mean net energy and net shortwave radiation are higher at Ganja La than at Yala during daytime in March, whereas there are negligible differences in the net energy and net shortwave radiation between the two sites during daytime in April and May. The net longwave radiation has a similar magnitude at both sites with less negative values in April and May than in February and March. Conversely, the magnitude of the latent heat flux shows distinct differences between the two sites. During the entire snow season the latent heat flux is considerably higher at Yala compared to Ganja La in the afternoon. This difference is largest in March, where the latent heat flux strongly reduces the net available energy at Yala. The sensible heat flux is a relatively small term compared to the other components of the energy balance and shows similar patterns for both Yala and Ganja La. During daytime the sensible heat flux is negligibly small, whereas the sensible heat flux increases during night, directing energy towards the snowpack, which is most evident in February and March.

4.3. Energy and mass balance experiments

The results of the different energy and mass balance experiments are summarized in Table 2. These results are discussed in the Subsections 4.3.1–4.3.4 below.

4.3.1. Melt

Snowmelt dominates the seasonal mass and energy balance at both sites, regardless of the experiment (Table 2). The seasonal melt estimate is highest for Exp. 1, i.e. 1201 mm/58 W m^{-2} and 1159 mm/43 W m^{-2} for Ganja La and Yala, respectively. The melt estimates are higher at

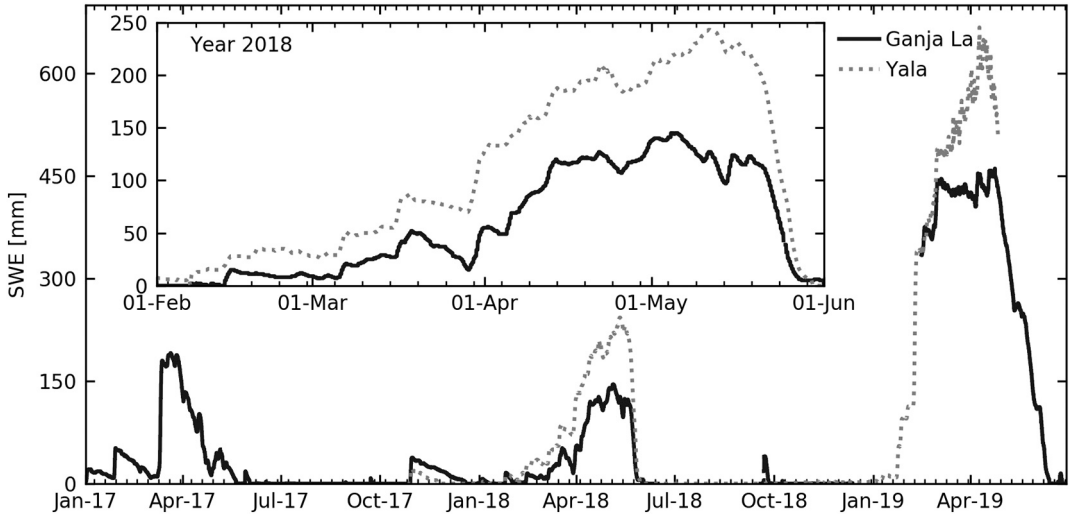

Fig. 2. Time series of the observed SWE from the CS725 SWE sensor at both Ganja La and Yala from January 2017 until June 2019. Note that the snow accumulation in January 2019 is not captured at Ganja La due to station failure. At Yala, SWE observations are only available from October 2017 until April 2019. Note that observed SWE at Yala exceeds the maximum reliable measurement range of 600 mm in April 2019. The inset shows the evolution of SWE in more detail for the 2018 snow season.

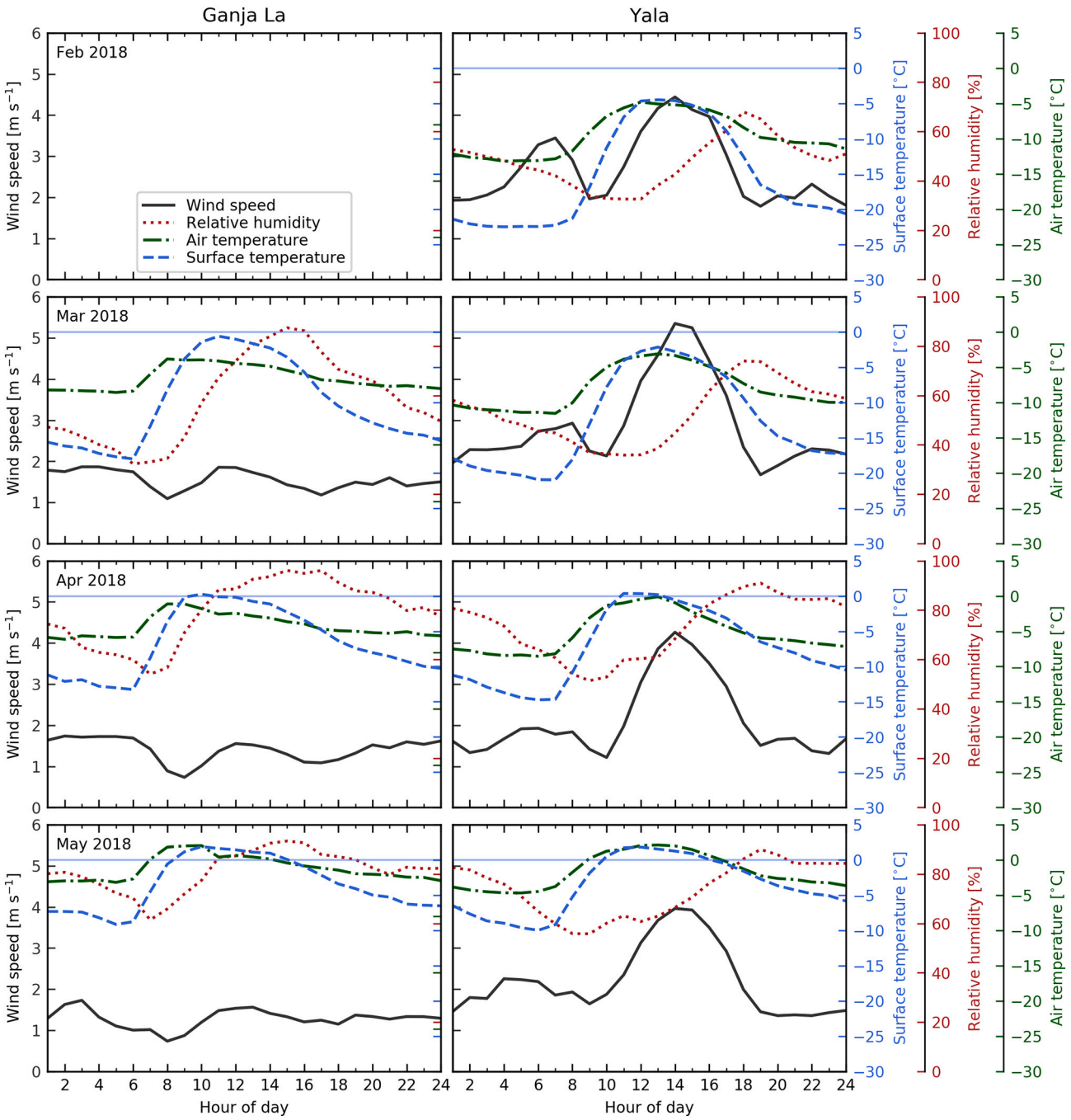

Fig. 3. Monthly averaged observed wind speed, air temperature, surface temperature and relative humidity at both Yala and Ganja La from February to May 2018 when sufficient snow is present (SWE > 15 mm). Snow is not sufficiently present to show the monthly averaged variables at Ganja La in February. The blue horizontal line indicates the zero-degrees line.

Ganja La compared to Yala (Table 2) and are very sensitive to the net shortwave radiation and hence the albedo of the snowpack. Table 3 shows the sensitivity of the melt estimates to the (chosen) albedo at Ganja La and Yala. The cumulative seasonal melt estimates almost double when assuming an albedo of 0.5 instead of 0.7. For an assumed albedo of 0.9, the major part of the incoming shortwave radiation is reflected resulting in only 67 mm and 60 mm of melt (Table 3).

Table 2 also shows a strong interannual variability in melt at Ganja La. The melt is estimated to be 976 mm in 2017, whereas it is 685 mm and 1066 mm in 2018 and 2019, respectively, according to Exp. 4.

4.3.2. *Refreezing*

The seasonal refreezing is moderately higher at Ganja La compared to Yala for Exp. 3 and Exp. 4 (Table 2). The refreezing estimates in Exp. 3 are higher than in Exp. 4, with increases of 119 and 134 mm at Ganja La and Yala, respectively. This leads to a higher fraction of meltwater that refreezes at Ganja La and Yala for Exp. 3 (0.49 and 0.59, respectively) than for Exp. 4 (0.32 and 0.34, respectively). The refreezing has a strong seasonality and is most substantial in April and May for Exp. 4 (Table 2). The refreezing estimates in Exp. 3 are energy limited, whereas the refreezing estimates in Exp. 4 can be either energy or water limited. We used the concept of the Budyko curve to determine whether refreezing is energy or water limited. The Budyko curve normally describes the

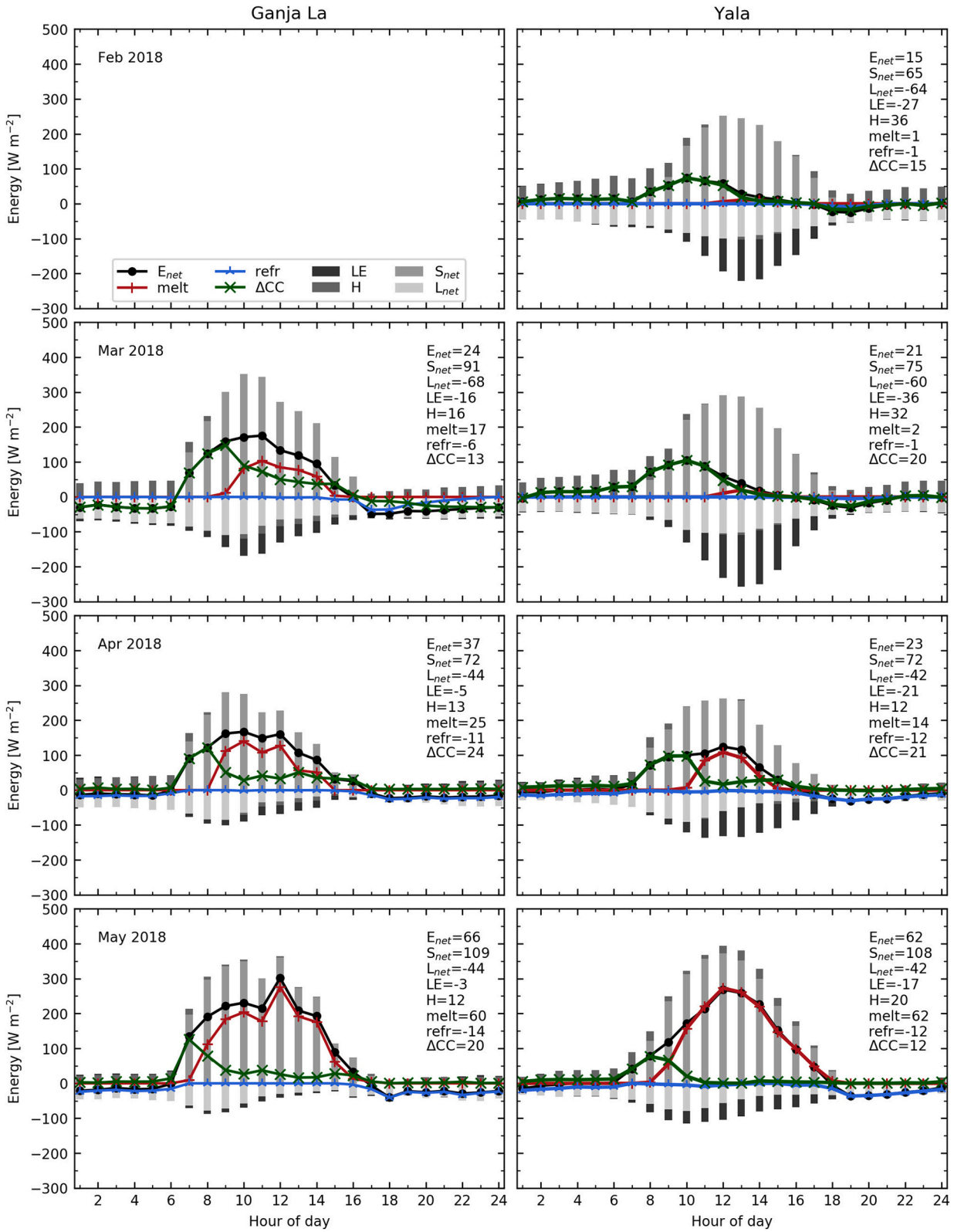

Fig. 4. Hourly energy balance, including the net shortwave (S_{net}) and net long wave (L_{net}) radiation, latent heat flux (LE) and the sensible heat flux (H). S_{net} and L_{net} are observed values and LE and H are calculated using the bulk-aerodynamic method. The net energy (E_{net}) is the sum of S_{net}, L_{net}, LE and H. Fluxes pointing towards the surface are assumed positive whereas fluxes pointed towards the atmosphere are negative. In addition, the figure illustrates the partitioning of E_{net} over the changes in cold content (ΔCC) of the snowpack (note that a positive ΔCC reduces the CC), melt or refreezing (*refr*). The partitioning of the net energy is based on Exp. 4 (explained in detail in Section 3.5). If $E_{net} > 0$ W m^{-2}, then E_{net} is partitioned over melt and decrease of the cold content, whereas E_{net} is partitioned over refreezing and increase of the cold content if $E_{net} < 0$ W m^{-2}. The monthly averaged values of all energy balance components is given in the text of each panel. Snow is not sufficiently present to show the monthly averaged variables at Ganja La in February.

Table 2
Results of the different snowpack energy and mass balance experiments at Yala and Ganja La for the 2018 winter season. The experiment numbers refer to the experiments described in Section 3.5. Please note that a positive Δ cold content reduces the cold content of the snowpack. The mass balance is defined as the sum of melt, refreezing, evaporation, sublimation and deposition in which negative values indicate mass losses and positive values indicate mass gains. The evaporation, sublimation and deposition are given in Table 4 since these values are constant across the experiments. The results of Exp. 4 are also given for the snow seasons 2017 and 2019 at Ganja La. However, note that the snow accumulation in January 2019 is not captured due to station failure.

		Ganja La				Yala			
		Melt [mm]/ [W m^{-2}]	Refreezing [mm]/ [W m^{-2}]	Δ cold content [W m^{-2}]	Mass balance [mm]	Melt [mm]/ [W m^{-2}]	Refreezing [mm]/ [W m^{-2}]	Δ cold content [W m^{-2}]	Mass balance [mm]
Exp. 1	Feb	–	–	–	–	−113/24	–	–	−128
	Mar	−322/47	–	–	−335	−259/32	–	–	−293
	Apr	−382/49	–	–	−387	−280/36	–	–	−300
	May	−498/80	–	–	−500	−506/76	–	–	−521
2018	**Total**	**−1201/58**	**–**	**–**	**−1222**	**−1159/43**	**–**	**–**	**−1242**
Exp. 2	Feb	–	–	–	–	−6/1	–	14	−21
	Mar	−119/17	–	7	−132	−15/2	–	19	−49
	Apr	−192/25	–	12	−197	−108/14	–	9	−128
	May	−374/60	–	6	−376	−418/62	–	0	−432
2018	**Total**	**−685/33**	**–**	**9**	**−705**	**−547/20**	**–**	**11**	**−631**
Exp. 3	Feb	–	–	–	–	−6/1	41/9	22	20
	Mar	−119/17	158/23	30	25	−15/2	92/11	30	43
	Apr	−192/25	93/12	25	−104	−108/14	99/13	22	−29
	May	−374/60	87/14	20	−288	−418/62	89/13	13	−344
2018	**Total**	**−685/33**	**338/16**	**25**	**−367**	**−547/20**	**320/12**	**22**	**−310**
Exp. 4	Feb	–	–	–	–	−6/1	5/1	15	−17
	Mar	−119/17	44/6	13	−88	−15/2	7/1	20	−41
	Apr	−192/25	87/11	24	−111	−108/14	89/12	21	−39
	May	−374/60	86/14	20	−289	−418/62	82/12	12	−350
2018	**Total**	**−685/33**	**219/11**	**19**	**−486**	**−547/20**	**186/7**	**18**	**−445**
2019	**Total**	**−1066/36**	**284/−10**	**22**	**−807**				
2017	**Total**	**−976/36**	**236/−10**	**10**	**−691**				

Table 3
Estimated melt and refreezing based on Exp. 4 with differing albedo at Ganja La and Yala for the 2018 snow season. 'Station' refers to the observed albedo at the AWSs, whereas 'Albedo 0.9','Albedo 0.7′ and 'Albedo 0.5′ refer to an assumed seasonal constant albedo of 0.9, 0.7 and 0.5, respectively.

	Melt / Refreezing [mm]			
	Station	Albedo 0.9	Albedo 0.7	Albedo 0.5
Ganja La				
Mar	−119/44	−2/2	−66/41	−160/50
Apr	−192/87	−12/11	−170/84	−343/85
May	−374/86	−53/44	−267/88	−490/84
Total	**−685/219**	**−67/59**	**−503/216**	**−993/221**
Yala				
Feb	−6/5	0/0	−2/2	−14/6
Mar	−15/7	−1/0	−15/8	−39/11
Apr	−108/89	−4/4	−118/77	−254/74
May	−418/82	−55/49	−293/80	−559/72
Total	**−547/186**	**−60/54**	**−428/167**	**−866/164**

theoretical energy and water limits of a catchment water balance by calculating the ratio of actual and potential evaporation over precipitation. Fig. 5 shows the adapted Budyko curves (ratio of actual and potential refreezing over melt) for Ganja La and Yala, which illustrate that refreezing (based on Exp. 4) is water limited in February and March (weeks 6–12), whereas refreezing is energy-limited in April and May (weeks 13–21).

Table 3 also shows the sensitivity of refreezing to the liquid water availability. A difference in albedo of 0.9 and 0.7 gives a large difference in refreezing as melt increases for a lower albedo and so does the liquid water content in the snowpack and the potential for refreezing. However, a difference in albedo of 0.7 and 0.5 does not result in any substantial difference in refreezing (Table 3).

4.3.3. Cold content

Table 2 shows the average monthly and seasonal cold content changes which were calculated as a residual energy of the surface energy balance for the Exp. 2–4. The seasonal averaged ΔCC is positive, with values ranging between 9 and 25 W m^{-2}, for all experiments. This means that the cold content of the snowpack is reduced and that the energy is used to warm the snowpack. Exp. 3 gives the highest averaged positive values as all negative energy at the snow surface is directed to refreezing in this experiment as water availability is assumed to be unlimited. As a result only positive ΔCC, which warm the snowpack and reduce the cold content, are included in the average value.

4.3.4. Mass balance

The observed seasonal cumulative increase in SWE is higher at Yala (334 mm) than at Ganja La (275 mm), most of which occurs in March and April (Table 4). Snowpack ablation is most substantial in May at both sites (Table 4). The latent heat flux is considerably higher at Yala, resulting in larger mass losses due to evaporation and sublimation at this site. The deposition is approximately equal at the two sites and has a negligible influence on the mass balance (Table 4). The mass balance does not close for all experiments at both locations, except for Exp. 3 at the Yala site, with only 24 mm difference between observation and calculation of the mass balance. In all other cases, the calculated mass loss for the experiments exceeds the observed mass loss. The overestimation of mass loss is logically largest for Exp. 1, at 966 and 908 mm respectively for Ganja La and Yala.

The interannual variability in accumulation is large at Ganja La. The cumulative increase in SWE in both 2017 and 2019, 364 mm and 737 mm, respectively, are higher than in 2018. The combined loss of snow

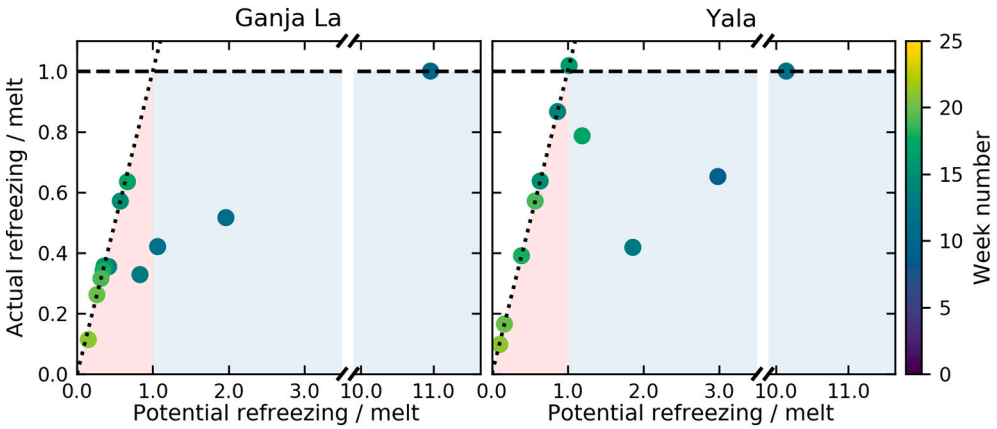

Fig. 5. Adjusted Budyko curves for Yala and Ganja La for the time period February-May 2018 when sufficient snow is present (SWE > 15 mm). The blue shaded area indicates the liquid water limit, whereas the red shaded area indicates the energy limit. The refreezing and melt estimates were aggregated to weekly values. The markers are colored to the according week number of the year. The potential refreezing is based on the results of Exp. 3, whereas the actual refreezing is based on the results of Exp. 4. Weeks without melt are excluded (weeks 6–8, 10 and 11 for Yala).

Table 4
Seasonal evaporation (Evap), sublimation (Subl), deposition (Dep) as calculated with the bulk-aerodynamic method for the 2018 winter season at the locations Ganja La and Yala. The seasonal cumulative increase and decrease of SWE are based on the CS725 SWE observations. Values are also given for the snow seasons 2017 and 2019 at Ganja La. However, note that the snow processes are not captured in January 2019 due to station failure.

	Ganja La					Yala				
	Evap [mm]/ [W m^{-2}]	Subl [mm]/ [W m^{-2}]	Dep [mm]/ [W m^{-2}]	Cumulative decrease SWE [mm]	Cumulative increase SWE [mm]	Evap [mm]/ [W m^{-2}]	Subl [mm]/ [W m^{-2}]	Dep [mm]/ [W m^{-2}]	Cumulative decrease SWE [mm]	Cumulative increase SWE [mm]
Feb	–	–	–	–	–	−1/−2	−15/−26	1/1	−14	27
Mar	−3/−4	−11/−13	1/1	−45	84	−1/−1	−35/−36	2/2	−28	133
Apr	−3/−3	−5/−5	3/3	−35	120	−6/−5	−16/−18	2/2	−47	127
May	−1/−2	−3/−4	3/4	−177	52	−8/−9	−9/−11	2/3	−246	47
Total	**−8/−3**	**−19/−8**	**6/2**	**−256**	**256**	**−16/ −4**	**−74/−23**	**6/2**	**−334**	**334**
2019	**−4/−1**	**−32/−9**	**10/3**	**−737**	**737**					
2017	**−11/−3**	**−44/−15**	**4/1**	**−364**	**364**					

due to evaporation and sublimation is two times higher in 2017 compared to 2018. The mass balance closes most in 2019 with only 70 mm difference between observation and calculation based on Exp. 4. This gap is larger in 2017 and 2018, at 327 and 230 mm, respectively.

4.4. Observed snowpack temperature and change in cold content

Figs. 6 and 7 show the transition of a cold snowpack in winter and early spring to an isothermal snowpack towards the end of the snow season in May. The temperature at the bottom of the snowpack shows no diurnal cycles, whilst the snow temperature closer to the surface shows a diurnal cycle with a minimum temperature of ~ − 11 °C around 5 h and a maximum of −2 °C around 13 h at the end of March (Fig. 6). This diurnal cycle becomes smaller towards the end of the snow season when the snowpack becomes isothermal, with the snow temperature varying between approximately −4 °C and 0 °C. At the end of the snow season the temperature sensor shows above zero temperature close to the snow-atmosphere interface, due to the influence of solar radiation. The diurnal cycle in snow temperature is a direct indication for the diurnal cycles in cold content. The cold content of the snowpack ranges between 0 and

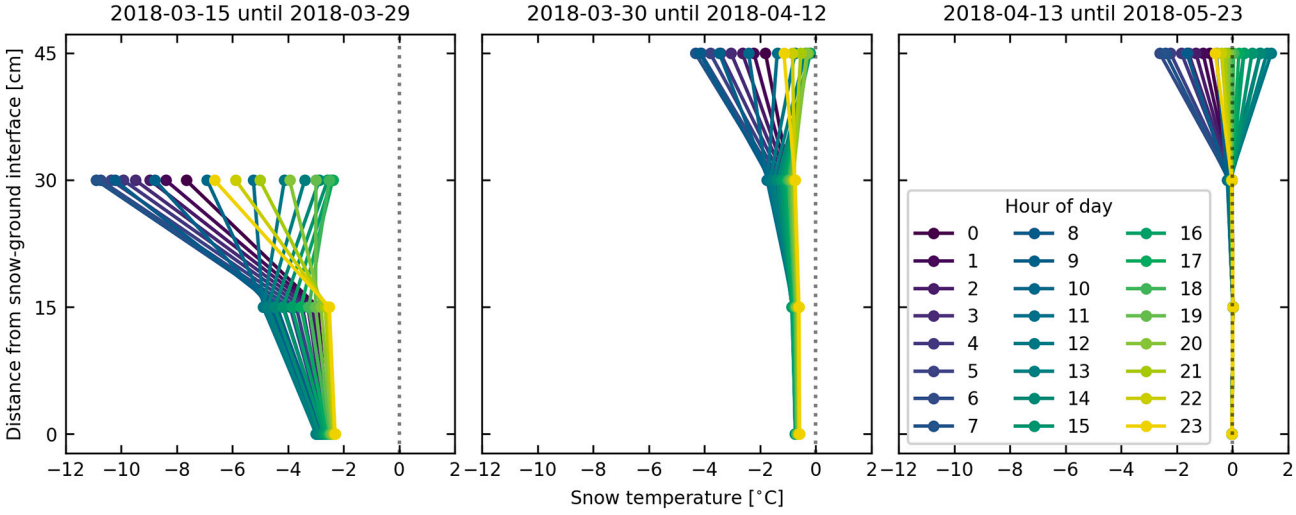

Fig. 6. Hourly vertical temperature profiles of the snowpack measured with the TidbiTs at Yala, averaged over three different time periods.

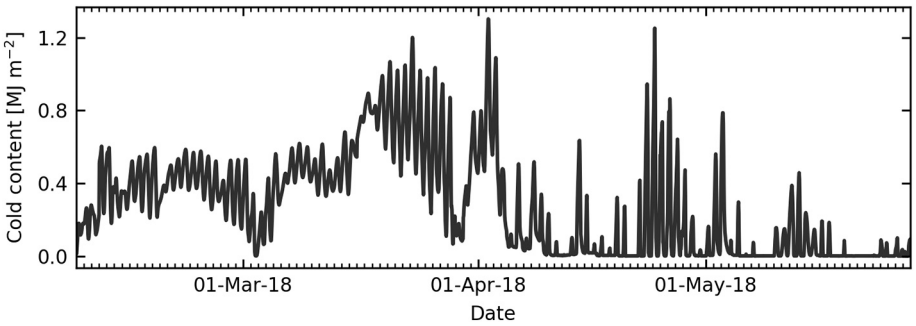

Fig. 7. The development of the observed cold content of the snowpack throughout the snow season 2018 at Yala.

1.2 MJ m^{-2} (Fig. 7). In February there is first a gradual increase of the cold content followed by a gradual decrease. The data also shows more abrupt changes in cold content, which are related to precipitation events, on 6–7 March, 15–16 March and 30–31 March 2018. From 9 April onwards the snowpack is isothermal during the day, but some cold content develops during the night.

5. Discussion

5.1. Meteorological drivers of the surface energy balance

During daytime hours, the net energy is generally more positive at Ganja La compared to the Yala site (Fig. 4). This is caused by a higher net shortwave radiation at Ganja La due to a lower albedo, which may be partially caused by larger boulders protruding from the snowpack as the snowpack is typically shallower at this site. The surface energy balance is most dominantly influenced by the net shortwave radiation. This is in consensus with the findings of Litt et al. (2019), who studied the contribution of the different surface energy balance components to melt for two glaciers in the Nepalese Himalaya.

Sublimation and evaporation are more pronounced at Yala, effectively reducing the net energy (Fig. 4) and lowering the surface temperature (Fig. 3). The higher latent heat flux at Yala is linked to the lower atmospheric humidity and higher wind speeds observed at Yala compared to Ganja La between 10 and 15 h, which is the moment that the latent heat flux typically peaks (Reba et al., 2012; Sexstone et al., 2018; Stigter et al., 2018). The differences in wind speed are likely related to the different aspects of each catchment. Ganja La is located at the end of a north-south oriented valley whereas Yala is located in the middle of an east-west oriented valley (Fig. 1), resulting in different wind regimes. Fig. 3 shows that the relative humidity increases at approximately 10 h at Ganja La, whereas this only increases at approximately 13–14 h at Yala where stronger winds result in stronger mixing. In contrast to the latent heat flux, the sensible heat flux is on average positive at both sites (Fig. 4), warming the snowpack, with highest values during night when the difference between the temperature of the snow surface and near surface air temperature is largest (Fig. 3). This is mainly observable in February and March at Yala. During the night, the positive sensible heat flux is (partly) offset by the negative net longwave radiation, resulting in a slightly negative or zero net energy (Fig. 4).

5.2. Energy and mass balance experiments

5.2.1. Melt

The melt estimates are very sensitive to the assumption under which snowmelt conditions occur. In Exp. 1 it was assumed that melt occurs once the net energy is positive. In the other experiments melt only occurred when the snow surface was observed to be at melting point in addition to available positive net energy. The seasonal melt estimates, without accounting for the cold content of the snow, are 2.1 and 1.8 times higher for Yala and Ganja La, respectively (Table 2). The melt estimates in Exp. 1 (1159 mm and 1201 mm) are unreasonably high compared to the observed seasonal cumulative decreases in SWE, i.e. 334 mm and 256 mm for Yala and Ganja La, respectively (Table 4). This shows that it is essential to include a threshold on the surface temperature when calculating melt based on the surface energy balance. The large difference between the calculated melt in Exp. 1 and the observed decrease in SWE also indicates that a large part of the net positive energy is likely used to overcome the cold content of the snowpack. The melt estimates are primarily driven by the net shortwave radiation, which in turn is highly sensitive to the albedo of the snowpack (Table 3). This is because the incoming shortwave radiation is relatively high in the Nepalese Himalaya due to the high altitude and low latitude compared with other mountain ranges in the world. An albedo of 0.7 halves the melt compared to using a value of 0.5, decreasing to just 7% when it is increased further to 0.9. The sensitivity of the surface energy balance to albedo is in consensus with previous studies on high-altitude Himalayan glaciers (Litt et al., 2019; Matthews et al., 2020). Indeed, the mass balance of Himalayan glaciers is most sensitive to variations in shortwave radiation and albedo (Azam et al., 2014; Kayastha et al., 1999). Results from this snowpack study and previous glacier studies indicate that future snow and ice melt estimates based on the surface energy balance should – in the absence of observations – carefully choose an albedo parameterization and account for its uncertainties.

Most of the seasonal melt occurs at the end of the snow season in May at both sites (Fig. 4 and Table 2). 374 mm and 418 mm of snow melts in May, which is 55% and 76% of total melt at Ganja La and Yala, respectively. In May, an increased amount of energy is available for melt at both sites. This is caused by i) increased net shortwave radiation due to decreasing albedo, ii) decreased latent heat flux due to increased atmospheric humidity and iii) less negative net longwave radiation due to more incoming radiation because of higher air temperature and increased atmospheric humidity. Note that at Yala the sensible heat flux also increases during daytime in May (Fig. 4), which may be (partly) caused by the development of a patchy snow cover and consequently higher air temperature due to heat advection from non-snow-covered areas (Mott et al., 2011; Schlögl et al., 2018; Shook and Gray, 1997). Even though this process is minor compared to the increase in net shortwave radiation at Yala, it does increase the melt rates. This effect is less apparent at Ganja La due to the lower wind speeds observed there.

5.2.2. Refreezing

Refreezing of meltwater in a snowpack can be either water limited or energy limited. Assuming unlimited water availability (Exp. 3) leads to 119 mm and 134 mm more refreezing than for the water limited case (Exp. 4) at Ganja La and Yala, respectively (Table 2). This indicates that refreezing is (partly) water limited. Especially in March the refreezing rate is significantly higher in Exp. 3 compared to Exp. 4 as net energy is negative during night, favorable for refreezing, but in Exp. 4 no meltwater is available to refreeze. Fig. 5 further illustrates when refreezing is energy or water limited. All data points located in the red and blue-

shaded areas indicate whether refreezing is energy or water limited, respectively. Fig. 5 demonstrates that refreezing is water limited at the start of the snow season (darker points), whereas refreezing becomes energy limited in spring (lighter points). The point just above the water limit at Yala means there is more refreezing than the actual meltwater produced during that week. The additional liquid water availability for refreezing can be explained by meltwater storage within the snowpack of the previous week. Table 3 shows that albedo also indirectly influences the estimated refreezing as it determines how much meltwater is available for refreezing. Therefore, albedo is not only important to quantify melt, but also to quantify refreezing.

If refreezing occurs, a part of the positive net energy is used to melt previously frozen meltwater. Therefore, in cases where seasonal melt exceeds the observed decreases in SWE, refreezing is likely the process that closes the potential gap in the mass balance. The difference in mass balance closure between Exp. 3 and Exp. 4 (Table 2) suggests that the amount of refreezing is insufficient to close the gap when meltwater retention within the snowpack is limited to values reported in literature (Heilig et al., 2015; Mitterer et al., 2011; Samimi and Marshall, 2017; Wever et al., 2015). Bayard et al. (2005) observed the presence of a basal ice layer when the soil beneath a snowpack was frozen for two alpine sites in Switzerland. In their case winter melt occurred. The meltwater percolated throughout the snowpack but at the base of the snowpack the water could not infiltrate due to frozen soil, forming the basal ice layer. If infiltration actually happens in frozen soils, the meltwater can refreeze and contribute to the development of a basal ice layer (Marsh and Woo, 1984). We therefore hypothesize that refreezing may not only consist of meltwater retained within the snowpack, but also of refreezing of ponded meltwater at the snowpack base. Ponding of meltwater at the snowpack base was observed at both Ganja La and Yala during fieldwork in April 2018. Kirkham et al. (2019) observed 3–4 ice lenses, each approximately 10 mm thick, within the snowpack (Fig. 8) and a basal ice layer of approximately 30 mm w.e. present in 12 snow pits dug within the footprint of the CS725 SWE sensor at Ganja La on April 30th 2018. At some locations within the footprint, the basal ice layer had a thickness of up to 110 mm (Kirkham et al., 2019). This supports the idea of having substantial refreezing at the base of the snowpack besides refreezing within the snowpack itself. However, no basal ice layer was observed on April 25th 2018 in three snow pits within the footprint of the CS725 SWE sensor at Yala. Instead, the snow at the base of the snowpack was wet and each of the three snow pits contained 5 ice layers, 10–15 mm thick within the snowpack (Fig. 8). The difference in the presence of a basal ice layer at the two sites may be a result of thermal insulation of the snowpack. The accumulation is higher at Yala than at Ganja La (Fig. 2), resulting in stronger insulation of the meltwater at the bottom of the snowpack from surface energy inputs at Yala. Our bulk approach does not resolve the effect of thermal insulation on deeper layers. Therefore, refreezing of meltwater may be overestimated using a bulk approach under the conditions mentioned above. Nevertheless, a comparison of the observed ice layers with refreezing estimates based on Exp. 4 show that the estimated refreezing at Ganja La (131 mm) is within the range of the observed ice layers (60–140 mm) on 30th of April. The refreezing estimate (92 mm) slightly exceeds the observed ice layers (50–75 mm) at Yala on the 25th of April. However, refreezing does not necessarily result in ice layers only. For example, a 60 mm thick melt-freeze crust was present in snow pit 3 at a depth of 15–21 cm from the snow surface at Yala (Fig. 8). This indicates that the actual refreezing is more substantial than estimates based on ice layers only. The estimates of refreezing for Exp. 3 are substantially higher than observations, indicating that Exp. 4, which includes a water limit, captures the refreezing more realistically. The results of Exp. 4 show that 32% and 34% of the seasonal melt is melt of refrozen meltwater at Ganja La and Yala, respectively. This is comparable to a first-order approximation by Saloranta et al. (2019), who estimated that 34% of total snow meltwater refreezes at the Ganja La site and that 36% refreezes on average over the entire Langtang catchment. Samimi and Marshall (2017) measured values of 9% in a supraglacial snowpack in the Canadian Rocky Mountains during the ablation season. In their study the value is likely lower due to the presence of a deeper snowpack and percolation of meltwater to deeper parts that are more isolated from energy changes at the snow-atmosphere interface. In addition, they focused on the ablation season in which the supraglacial snowpack was mainly isothermal, reducing the refreezing. Besides the influence of refreezing on the mass balance, the melt of refrozen meltwater is an energy 'sink', consuming 19% and 16% of the total observed positive net energy at Ganja La and Yala, respectively. Refreezing is therefore a considerable component in the energy balance and mass balance of the seasonal snowpack in 2018. Again, the energy sink was measured to be 9% in the study of Samimi and Marshall (2017). At Ganja La, the seasonal refreezing was also calculated for 2017 and 2019. In these years the energy 'sink' is 17% and 16%, respectively, which is within the same range as in 2018. The percentage of meltwater that refreezes is also comparable in 2017 and 2019, at 24% and 27%, respectively, to 2018.

Besides temporal variability, refreezing will also vary spatially. For example, Ayala et al. (2017a) showed that refreezing is maximal at an elevation ranging between 4500 and 5000 m a.s.l in the Andes by using a distributed energy balance model. At higher altitude (>5000 m a.s.l.), refreezing is limited by available meltwater. At lower elevations (4500 m a.s.l.) refreezing is limited to available water, but this is caused by a shallower snowpack and therefore small liquid water storage capacity (Ayala et al., 2017a). For this reason refreezing is also reduced during the ablation season when the snow depth becomes smaller (Ayala et al., 2017b). Saloranta et al. (2019) showed that refreezing is most substantial at an altitude ranging between 5000 m and 6000 m a.s.l. in the

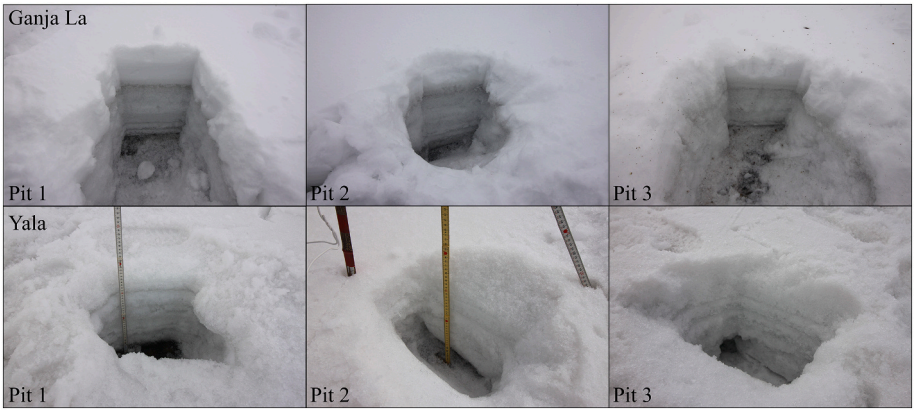

Fig. 8. Pictures of three snow pits at Ganja La on April 30th 2018 and Yala on April 25th 2018. The snow pits at Ganja La have a depth of 41–42 cm and contain four or five ice layers. The snow pits at Yala have a depth of 38–44 cm and contain five ice layers.

Langtang catchment. Future work should focus on quantifying refreezing in space using an energy balance-approach.

5.2.3. Cold content

The seasonal averaged change in cold content (including both positive and negative changes) is only 1 W m^{-2}, based on the observed vertical snow temperature profile at Yala. This appears small compared to the other components of the energy balance. However, the positive and negative changes in the cold content balance each other out. The seasonal average decrease in cold content of the snowpack (positive changes only) was estimated to be 9 W m^{-2}. This means that, on average, 9 W m^{-2} of the net positive energy is used to reach an isothermal snowpack and initiate melt onset. This energy flux is substantial since the total net positive energy available in February-May 2018 is on average 43 W m^{-2} (Fig. 4). The large fraction of positive energy used (21%), is caused by the strong diurnal cycles of warming during daytime and cooling overnight (Fig. 6). This illustrates that it is key to account for the daily cycles of the cold content in energy balance based snowmelt models. This has also been shown by the difference in the melt estimate between Exp. 1 and the other experiments (Table 2).

The observed cold content of the snowpack at Yala shows a regular diurnal cycle, but also a few abrupt step-wise increases unrelated to the daily cycle (Fig. 7). These sudden increases in the cold content of the snowpack on 6–7 March, 15–16 March and 30–31 March 2018 coincide with substantial increases of SWE due to snowfall, i.e. 20 mm, 28 mm and 46 mm, respectively. Jennings et al. (2018) showed that precipitation is the primary source for cold content additions to the snowpack for an alpine snowpack in the Colorado Rocky Mountains. The secondary source in this study is a negative surface energy balance. According to Jennings et al. (2018), three main approaches exist to estimate the cold content of a snowpack, namely: i) as an empirical function of cumulative air temperature, ii) as an empirical function of cumulative precipitation and corresponding temperature (which is often assumed equal to the air temperature), and iii) as a residual of the surface energy balance. As the observed cold content in our study shows both diurnal cycles and abrupt increases, this indicates that the cold content is influenced by both cold content gains from snowfall and from the surface energy balance residuals (Fig. 7). Nonetheless, no (statistically significant) relation was found between changes in the observed cold content of the snowpack and increases in SWE (following the above-mentioned method ii) or between changes in the cold content of the snowpack and surface energy balance residuals (taken from Exp. 4). This can be (partly) explained by the different climate in the study of Jennings et al. (2018). For example, there is more accumulation of SWE and also the surface energy balance is less driven by shortwave radiation than at Yala. Longer observational time series are required to investigate whether the relations shown by Jennings et al. (2018) also hold for the climate in the Central Himalaya.

5.3. Closure of the mass and energy balances

We hypothesize that the results of Exp. 4 should get closest to the observations as it includes melt, the cold content and water limited refreezing. The sum of estimated melt, refreezing, evaporation, sublimation and deposition (disregarding erosion by wind) should match the observations of cumulative decrease in SWE over the entire snow season. However, the observations show a seasonal decrease of SWE of 256 mm (Ganja La) and 334 mm (Yala), whereas the results of Exp. 4 show mass losses of 486 mm and 445 mm, respectively (Tables 2 and 4). This is a substantial difference. Exp. 3 closes the mass balance most due to more refreezing as there is unlimited water availability for refreezing when the net energy is negative (Tables 2 and 4). The snow pit observations show that the estimated refreezing in Exp. 4 matches the observed ice layers both within and at the base of the snowpack. Nevertheless, the actual refreezing exceeds these observations as refreezing does not necessarily result in ice layers only. This indicates that Exp. 4 may represent the lower boundary of refreezing estimates. The actual refreezing is likely within the range of the estimates of Exp. 3 and Exp. 4. The remaining gap in the mass balance is due to nonclosure of the energy balance. This nonclosure of the energy balance is visible in the estimates of the seasonal averaged change in cold content according to Exp. 4, i.e. 18 W m^{-2} at Yala (Table 2). This value is considerably higher than the observation based estimate of 1 W m^{-2} (described in Section 5.2.3) and suggests a positive imbalance of 17 W m^{-2} in seasonal mean measured energy at Yala. That mass and energy balance do not close has been reported before for seasonal snow cover overlying frozen soils (e.g. Helgason and Pomeroy, 2012a; Pan et al., 2017). Several reasons could explain the imbalance in our study. Firstly, the surface energy balance is highly dependent on the incoming shortwave radiation and albedo (Table 3). A small measurement error in either the incoming shortwave radiation or albedo could result in the observed gap in the energy and mass balance. Secondly, and related to the previous argument, the melt estimates are sensitive to the assumed threshold value of SWE (15 mm) for the presence of snow. Thirdly, heat advection of precipitation was not included and is likely a minor term, increasing the cold content of the snowpack. Fourthly, the ground heat flux was not accounted for and can be a potential source or sink of energy (Granger and Male, 1978; Helgason and Pomeroy, 2012a). Yet, no adequate observations exist in the Himalaya to quantify the potential magnitude of this flux and only few observations exist elsewhere. Fifthly, there are uncertainties related to the calculated turbulent fluxes (e.g. Foken, 2008; Helgason and Pomeroy, 2012a, 2012b). However, the magnitude of turbulent fluxes is generally smaller than the radiative components. Helgason and Pomeroy (2012a) concluded that their energy imbalance could be closed with an unmeasured windless sensible heat exchange, but this process remains poorly understood. Besides uncertainties in the quantification of snow processes that influence the snowpack mass balance, there are also uncertainties in the observed SWE. The observed peak SWE is below 300 mm at both sites in the 2018 winter season, which is analyzed here. Therefore, a 15 mm uncertainty estimate applies (Section 3.2). In addition, uncertainty in the observed SWE may arise from the relatively large measurement interval of the CS725. The CS725 measures over a 24-h window, which is reported every 6 h. Increases and decreases of SWE within the 24-h interval may balance out. However, these sources of uncertainty are virtually impossible to quantify.

6. Conclusions

In this study, based on unique high-altitude snow and meteorological observations, the link between the observed energy balance and snowmelt, refreezing and cold content of the snowpack was systematically addressed and the following key conclusions can be drawn:

In a Himalayan setting with its high altitude, relatively low latitude and limited cloud cover during the melt season, the net energy for snow processes is primarily driven by the net shortwave radiation. This makes melt models and estimates highly sensitive to the snow albedo and potential measurement errors in shortwave radiation. Subtle spatial differences in net energy are likely linked to different wind and humidity patterns and the associated magnitude of turbulent fluxes.

The amount of net positive energy during February until May in 2018 is approximately two times larger than what is required to melt the snowpack at both sites considered. This illustrates the importance of accounting for the cold content of the snowpack and the refreezing process.

The experimental results show that refreezing plays a critical role in both the energy and mass balance of the snowpack. In case of unlimited liquid water in the snowpack, 49% and 59% of the melt refreezes again for Ganja La and Yala, respectively. In the case when water is limited this amount reduces to 32% and 34%, respectively.

A considerable amount of positive net energy (21%) is used to overcome the nightly increase in cold content and achieve the 0 °C isotherm conditions to initiate melt during the day at one of the locations, which is based on observed snow temperature profiles. Analysis of

surface energy balance residuals showed that, with the exception of May, when the snowpack is largely isothermal, this amounts up to 50% at both considered locations.

The mass and energy balance is not entirely closed. Even considering the cold content and refreezing, there is still more energy available than what is required to melt the snowpack. Possible explanations, which require further study, are uncertainties in the measurements of shortwave radiation, the observed albedo and possible sinks of energy which are not considered such as refreezing of a ponded water/ice layer at the soil-snow interface, an increase in cold content by fresh snowfall and the ground heat flux.

Author contribution

ES and WI designed the study with inputs from JS and IK. ES conducted the analysis and calculations. ES wrote the initial version of the manuscript with inputs from WI. All authors contributed to the final version of the manuscript. Also, all authors participated in field work and data collection.

Funding

Netherlands Organization for Scientific Research NWO; European Research Council; ICIMOD's Cryosphere Initiative (which is funded by Norway and by core funds contributed by the Governments of Afghanistan, Australia, Austria, Bangladesh, Bhutan, China, India, Myanmar, Nepal, Norway, Pakistan, Sweden, and Switzerland).

Data availability

The data can be shared upon request to the corresponding author.

Declaration of Competing Interest

The authors declare that they have no conflict of interest.

Acknowledgement

We acknowledge Mark Eijkelboom for designing and constructing the vertical snow temperature profile set-up. We would also like to acknowledge Tom Matthews for helpful discussions on the snowpack energy balance closure at high altitude in the Himalaya. We thank members of ICIMOD's Cryosphere Initiative, all porters and guides from Thamserku and Glacier Safari Trekking for their support in the field. The views and interpretations in this publication are those of the authors and are not necessarily attributable to ICIMOD. We also gratefully acknowledge the two anonymous reviewers and the editor Jukka Tuhkuri for providing comments that helped improve this manuscript.

References

Avanzi, F., De Michele, C., Morin, S., Carmagnola, C.M., Ghezzi, A., Lejeune, Y., 2016. Model complexity and data requirements in snow hydrology: seeking a balance in practical applications. Hydrol. Process. 30, 2106–2118. https://doi.org/10.1002/hyp.10782.

Ayala, A., Pellicciotti, F., Peleg, N., Burlando, P., 2017a. Melt and surface sublimation across a glacier in a dry environment: distributed energy-balance modelling of Juncal Norte Glacier, Chile. J. Glaciol. 63 (241), 803–822. https://doi.org/10.1017/jog.2017.46.

Ayala, A., Pellicciotti, F., MacDonell, S., McPhee, J., Burlando, P., 2017b. Patterns of glacier ablation across North-Central Chile: Identifying the limits of empirical melt models under sublimation-favorable conditions. Water Resour. Res. 53, 5601–5625. https://doi.org/10.1002/2016WR020247.

Azam, M.F., Wagnon, P., Vincent, C., Ramanathan, A.L., Favier, V., Mandal, A., Pottakkal, J.G., 2014. Processes governing the mass balance of Chhota Shigri Glacier (western Himalaya, India) assessed by point-scale surface energy balance measurements. Cryosphere 8 (6), 2195–2217. https://doi.org/10.5194/tc-8-2195-2014.

Bartelt, P., Lehning, M., 2002. A physical SNOWPACK model for the Swiss avalanche warning part I: numerical model. Cold Reg. Sci. Technol. 35, 123–145. https://doi.org/10.1016/S0165-232X(02)00074-5.

Bayard, D., Stähli, M., Parriaux, A., Flühler, H., 2005. The influence of seasonally frozen soil on the snowmelt runoff at two Alpine sites in southern Switzerland. J. Hydrol. 309 (1–4), 66–84. https://doi.org/10.1016/j.jhydrol.2004.11.012.

Bengtsson, L., 1982a. Percolation of meltwater through a snowpack. Cold Reg. Sci. Technol. 6, 73–81. https://doi.org/10.1016/0165-232X(82)90046-5.

Bengtsson, L., 1982b. The importance of refreezing on the diurnal snowmelt cycle with application to a northern Swedish catchment. Nord. Hydrol. 13 (1), 1–12. https://doi.org/10.2166/nh.1982.0001.

Bolch, T., Shea, J.M., Liu, S., Azam, F.M., Gao, Y., Gruber, S., Immerzeel, W.W., Kulkarni, A., Li, H., Tahir, A.A., Zhang, G., Zhang, Y., 2019. Status and change of the cryosphere in the extended Hindu Kush Himalaya region. In: The Hindu Kush Himalaya Assessment. Springer International Publishing, pp. 209–255.

Bookhagen, B., Burbank, D.W., 2010. Toward a complete Himalayan hydrological budget: Spatiotemporal distribution of snowmelt and rainfall and their impact on river discharge. J. Geophys. Res. Earth Surf. 115 (3), 1–25. https://doi.org/10.1029/2009JF001426.

Dingman, S.L., 2008. Physical Hydrology, 2nd ed. Waveland Press Inc.

Foken, T., 2008. The energy balance closure problem : an overview. Ecol. Appl. 18 (6), 1351–1367. https://doi.org/10.1890/06-0922.1.

Förster, K., Meon, G., Marke, T., Strasser, U., 2014. Effect of meteorological forcing and snow model complexity on hydrological simulations in the Sieber catchment (Harz Mountains, Germany). Hydrol. Earth Syst. Sci. 18 (11), 4703–4720. https://doi.org/10.5194/hess-18-4703-2014.

Fujita, K., Ageta, Y., 2000. Effect of summer accumulation on glacier mass balance on the Tibetan Plateau revealed by mass-balance model. J. Glaciol. 46 (153), 244–252. https://doi.org/10.3189/172756500781832945.

Granger, R.J., Male, D.H., 1978. Melting of a prairie snowpack (Canada). J. Appl. Meteorol. 17 (2), 1833–1842. https://doi.org/10.1175/1520-0450(1978)017<1833:MOAPS>2.0.CO;2.

Heilig, A., Mitterer, C., Schmid, L., Wever, N., Schweizer, J., Marshall, H., Eisen, O., 2015. Seasonal and diurnal cycles of liquid water in snow — Measurements and modeling. J. Geophys. Res. Earth Surf. 120, 2139–2154. https://doi.org/10.1002/2015JF003593.

Helgason, W., Pomeroy, J., 2012a. Problems closing the energy balance over a homogeneous snow cover during midwinter. J. Hydrometeorol. 13 (2), 557–572. https://doi.org/10.1175/JHM-D-11-0135.1.

Helgason, W., Pomeroy, J.W., 2012b. Characteristics of the near-surface boundary layer within a mountain valley during winter. J. Appl. Meteorol. Climatol. 51 (3), 583–597. https://doi.org/10.1175/JAMC-D-11-058.1.

Immerzeel, W.W., Droogers, P., de Jong, S.M., Bierkens, M.F.P., 2009. Large-scale monitoring of snow cover and runoff simulation in Himalayan river basins using remote sensing. Remote Sens. Environ. 113 (1), 40–49. https://doi.org/10.1016/j.rse.2008.08.010.

Immerzeel, W.W., van Beek, L.P.H., Konz, M., Shrestha, A.B., Bierkens, M.F.P., 2012. Hydrological response to climate change in a glacierized catchment in the Himalayas. Clim. Chang. 110 (3–4), 721–736. https://doi.org/10.1007/s10584-011-0143-4.

Immerzeel, W.W., Petersen, L., Ragettli, S., Pellicciotti, F., 2014. The importance of observed gradients of air temperature and precipitation for modeling runoff from a glacierized watershed in the Nepalese Himalaya. Water Resour. Res. 50, 2212–2226. https://doi.org/10.1002/2013WR014506.

Jennings, K.S., Kittel, T.G.F., Molotch, N.P., 2018. Observations and simulations of the seasonal evolution of snowpack cold content and its relation to snowmelt and the snowpack energy budget. Cryosph. 12, 1595–1614. https://doi.org/10.5194/tc-12-1595-2018.

Kayastha, R.B., Ohata, T., Ageta, Y., 1999. Application of a mass-balance model to a Himalayan glacier. J. Glaciol. 45 (151), 559–567. https://doi.org/10.3189/S002214300000143X.

Kirkham, J.D., Koch, I., Saloranta, T.M., Litt, M., Stigter, E.E., Møen, K., Thapa, A., Melvold, K., Immerzeel, W.W., 2019. Near real-time measurement of snow water equivalent in the Nepal Himalayas. Front. Earth Sci. 7 (July), 1–18. https://doi.org/10.3389/feart.2019.00177.

Lievens, H., Demuzere, M., Marshall, H., Reichle, R.H., Brangers, I., De Rosnay, P., Dumont, M., Girotto, M., Walter, W., 2019. Snow depth variability in the Northern Hemisphere mountains observed from space. Nat. Commun. 1–33 https://doi.org/10.1038/s41467-019-12566-y.

Litt, M., Shea, J., Wagnon, P., Steiner, J., Koch, I., Stigter, E., Immerzeel, W., 2019. Glacier ablation and temperature indexed melt models in the Nepalese Himalaya. Sci. Rep. 9 (1), 1–13. https://doi.org/10.1038/s41598-019-41657-5.

Litt, M., Sicart, J.E., Helgason, W.D., Wagnon, P., 2015. Turbulence characteristics in the atmospheric surface layer for different wind regimes over the tropical Zongo Glacier (Bolivia, 16° S). Bound. Layer Meteorol. 154 (3), 471–495. https://doi.org/10.1007/s10546-014-9975-6.

Marks, D., Dozier, J., 1992. Climate and energy exchange at the snow surface in the Alpine Region of the Sierra Nevada: 2. Snow cover energy balance. Water Resour. Res. 28 (11), 3043–3054. https://doi.org/10.1029/92WR01483.

Marsh, P., Woo, M.-K., 1984. Wetting front advance and freezing of meltwater within a snow cover: 1. Observations in the Canadian Arctic. Water Resour. Res. 20 (12), 1853–1864. https://doi.org/10.1029/WR020i012p01853.

Matthews, T., Perry, L.B., Koch, I., Aryal, D., Khadka, A., Shrestha, D., Abernathy, K., Elmore, A.C., Seimon, A., Tait, A., Elvin, S., Tuladhar, S., Baidya, S., Potocki, M., Birkel, S.D., Kang, S., Sherpa, T.C., Gajurel, A., Mayewski, P.A., 2020. Going to

extremes: installing the world's highest weather stations on Mount Everest. Bull. Am. Meteorol. Soc. 101 (11), E1870–E1890. https://doi.org/10.1175/bams-d-19-0198.1.
Mitterer, C., Hirashima, H., Schweizer, J., 2011. Wet-snow instabilities: Comparison of measured and modelled liquid water content and snow stratigraphy. Ann. Glaciol. 52 (58), 201–208. https://doi.org/10.3189/172756411797252077.
Mölg, T., Maussion, F., Yang, W., Scherer, D., 2012. The footprint of Asian monsoon dynamics in the mass and energy balance of a Tibetan glacier. Cryosphere 6 (6), 1445–1461. https://doi.org/10.5194/tc-6-1445-2012.
Mott, R., Egli, L., Grünewald, T., Dawes, N., Manes, C., Bavay, M., Lehning, M., 2011. Micrometeorological processes driving snow ablation in an Alpine catchment. Cryosph. 5, 1083–1098. https://doi.org/10.5194/tc-5-1083-2011.
Pan, X., Helgason, W., Ireson, A., Wheater, H., 2017. Field-scale water balance closure in seasonally frozen conditions. Hydrol. Earth Syst. Sci. 21 (11), 5401–5413. https://doi.org/10.5194/hess-21-5401-2017.
Pfeffer, W.T., Humphrey, N.F., 1998. Formation of ice layers by infiltration and refreezing of meltwater. Ann. Glaciol. 26, 83–91. https://doi.org/10.3189/1998aog26-1-83-91.
Pfeffer, W.T., Meier, M.F., Illangasekare, T.H., 1991. Retention of Greenland runoff by refreezing: implications for projected future sea level change. J. Geophys. Res. 96 (C12) https://doi.org/10.1029/91jc02502.
Ragettli, S., Pellicciotti, F., Immerzeel, W.W., Miles, E.S., Petersen, L., Heynen, M., Shea, J.M., Stumm, D., Joshi, S., Shrestha, A., 2015. Unraveling the hydrology of a Himalayan catchment through integration of high resolution in situ data and remote sensing with an advanced simulation model. Adv. Water Resour. 78, 94–111. https://doi.org/10.1016/j.advwatres.2015.01.013.
Reba, M.L., Pomeroy, J., Marks, D., Link, T.E., 2012. Estimating surface sublimation losses from snowpacks in a mountain catchment using eddy covariance and turbulent transfer calculations. Hydrol. Process. 26 (24), 3699–3711. https://doi.org/10.1002/hyp.8372.
Reijmer, C.H., Van Den Broeke, M.R., Fettweis, X., Ettema, J., Stap, L.B., 2012. Refreezing on the Greenland ice sheet: a comparison of parameterizations. Cryosphere 6 (4), 743–762. https://doi.org/10.5194/tc-6-743-2012.
Saloranta, T., Thapa, A., Kirkham, J.D., Koch, I., Melvold, K., Stigter, E.E., Litt, M., Møen, K., 2019. A model setup for mapping snow conditions in high-mountain Himalaya. Front. Earth Sci. 7, 129. https://doi.org/10.3389/feart.2019.00129.
Samimi, S., Marshall, S.J., 2017. Diurnal cycles of meltwater percolation, refreezing, and drainage in the supraglacial snowpack of Haig Glacier, Canadian Rocky Mountains. Front. Earth Sci. 5 (February), 1–15. https://doi.org/10.3389/feart.2017.00006.
Schlögl, S., Lehning, M., Mott, R., 2018. How are turbulent sensible heat fluxes and snow melt rates affected by a changing snow cover fraction? Front. Earth Sci. 6 (October), 1–13. https://doi.org/10.3389/feart.2018.00154.
Sexstone, G.A., Clow, D.W., Fassnacht, S.R., Liston, G.E., Hiemstra, C.A., Knowles, J.F., Penn, C.A., 2018. Snow sublimation in mountain environments and its sensitivity to forest disturbance and climate warming. Water Resour. Res. 54 (2), 1191–1211. https://doi.org/10.1002/2017WR021172.
Shea, J.M., Wagnon, P., Immerzeel, W.W., Biron, R., Brun, F., Pellicciotti, F., 2015a. A comparative high-altitude meteorological analysis from three catchments in the Nepalese Himalaya. Int. J. Water Resour. Dev. 31 (2), 174–200. https://doi.org/10.1080/07900627.2015.1020417.
Shea, J.M., Immerzeel, W.W., Wagnon, P., Vincent, C., Bajracharya, S., 2015b. Modelling glacier change in the Everest region, Nepal Himalaya. Cryosphere 9 (3), 1105–1128. https://doi.org/10.5194/tc-9-1105-2015.
Shook, K., Gray, D.M., 1997. Snowmelt resulting from advection. Hydrol. Process. 11 (13), 1725–1736. https://doi.org/10.1002/(SICI)1099-1085(19971030)11:13<1725::AID-HYP601>3.0.CO;2-P.
Smith, T., Bookhagen, B., 2018. Changes in seasonal snow water equivalent distribution in high mountain Asia (1987 to 2009). Sci. Adv. 4 (1) https://doi.org/10.1126/sciadv.1701550.
Smith, T., Bookhagen, B., Rheinwalt, A., 2017. Spatiotemporal patterns of High Mountain Asia's snowmelt season identified with an automated snowmelt detection algorithm, 1987-2016. Cryosphere 11 (5), 2329–2343. https://doi.org/10.5194/tc-11-2329-2017.
Steger, C.R., Reijmer, C.H., van den Broeke, M.R., Wever, N., Forster, R.R., Koenig, L.S., Kuipers Munneke, P., Lehning, M., Lhermitte, S., Ligtenberg, S.R.M., Miège, C., Noël, B.P.Y., 2017. Firn meltwater retention on the greenland ice sheet: a model comparison. Front. Earth Sci. 5 (January) https://doi.org/10.3389/feart.2017.00003.
Stigter, E.E., Wanders, N., Saloranta, T.M., Shea, J.M., Bierkens, M.F.P., Immerzeel, W.W., 2017. Assimilation of snow cover and snow depth into a snow model to estimate snow water equivalent and snowmelt runoff in a Himalayan catchment. Cryosph. 1647–1664.
Stigter, E.E., Litt, M., Steiner, J.F., Bonekamp, P.N.J., Shea, J.M., Bierkens, M.F.P., Immerzeel, W.W., 2018. The importance of snow sublimation on a Himalayan glacier. Front. Earth Sci. 6 (108), 1–16. https://doi.org/10.3389/FEART.2018.00108.
Van Pelt, W.J.J., Oerlemans, J., Reijmer, C.H., Pohjola, V.A., Pettersson, R., Van Angelen, J.H., 2012. Simulating melt, runoff and refreezing on Nordenskiöldbreen, Svalbard, using a coupled snow and energy balance model. Cryosphere 6 (3), 641–659. https://doi.org/10.5194/tc-6-641-2012.
van Pelt, W.J.J., Pohjola, V.A., Reijmer, C.H., 2016. The changing impact of snow conditions and refreezing on the mass balance of an idealized Svalbard Glacier. Front. Earth Sci. 4 (November), 1–15. https://doi.org/10.3389/feart.2016.00102.
Vionnet, V., Brun, E., Morin, S., Boone, A., Faroux, S., Le Moigne, P., Martin, E., Willemet, J.M., 2012. The detailed snowpack scheme Crocus and its implementation in SURFEX v7.2. Geosci. Model Dev. 5 (3), 773–791. https://doi.org/10.5194/gmd-5-773-2012.
Warscher, M., Strasser, U., Kraller, G., Marke, T., Franz, H., Kunstmann, H., 2013. Performance of complex snow cover descriptions in a distributed hydrological model system: a case study for the high Alpine terrain of the Berchtesgaden Alps. Water Resour. Res. 49, 2619–2637. https://doi.org/10.1002/wrcr.20219.
Wever, N., Schmid, L., Heilig, A., Eisen, O., Fierz, C., Lehning, M., 2015. Verification of the multi-layer SNOWPACK model with different water transport schemes. Cryosphere 9 (6), 2271–2293. https://doi.org/10.5194/tc-9-2271-2015.